THE JOURNAL OF PHYSICAL CHEMISTRY C

Article

pubs.acs.org/JPCC

Structure and Electronic Properties of a Continuous Random Network Model of an Amorphous Zeolitic Imidazolate Framework (a-ZIF)

Puja Adhikari,[†] Mo Xiong,[‡] Neng Li,[*,‡] Xiujian Zhao,[‡] Paul Rulis,[†] and Wai-Yim Ching[*,†]

[†]Department of Physics and Astronomy, University of Missouri—Kansas City, Kansas City, Missouri 64110, United States

[‡]State Key Laboratory of Silicate Materials for Architectures, Wuhan University of Technology, No. 122, Luoshi Road, Wuhan 430070, People's Republic of China

Supporting Information

ABSTRACT: Zeolitic imidazolate frameworks (ZIFs) are a rapidly emerging class of versatile porous material with many potential applications. Here, we report the construction of an amorphous ZIF (a-ZIF) model from a near-perfect continuous random network model of a-SiO_2. The radial distribution function is in good agreement with measurements for amorphous a_TZIF-4 but with notable fine differences. The electronic structure and properties of the a-ZIF model are critically compared with those of three crystalline ZIF phases, ZIF-4, ZIF-zni, and ZIF-8, using density functional theory methods. We confirm the retention of the metal tetrahedral bonding coordination in a-ZIF and the nearly identical short-range ordering found in crystalline ZIFs. The considerable Zn−N bond strength plays a key role in retaining the tetrahedrally bonded network structure. The calculated optical properties of a-ZIF show a complex absorption spectrum with an ultralow refractive index n of 1.327 and a plasmon frequency of 15.810 eV.

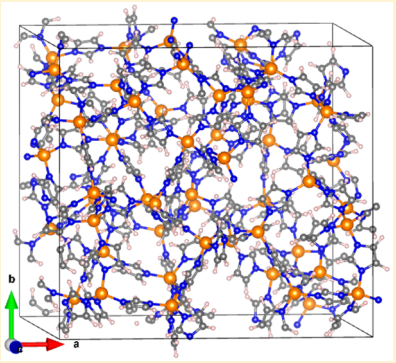

INTRODUCTION

Metal−organic frameworks (MOFs) have attracted immense attention from diverse disciplines of chemistry, physics, engineering, material sciences, biological and biomedical sciences.[1−4] An important member of the MOF family is the zeolitic imidazolate framework (ZIF), which display network topologies analogous to those of silica. In the network, the corner-sharing SiO_4 tetrahedra are replaced by MN_4 tetrahedra (M = metal, Zn in this work) linked by imidazolate (IM) $(C_3N_2H_3)^-$ anions (Figure 1a). The chemically tunable porosities of ZIFs are pivotal for their potential application in gas storage and separation, drug delivery, heterogeneous catalysis, and selective adsorption.[5−8] In addition to the large number of crystalline ZIFs with well-defined zeolite structures, the emerging category of noncrystalline or amorphous ZIF glasses obtained by melt-quenching the liquids that are formed upon melting of hybrid structures,[9] by transforming from crystalline phases by varying temperature[10,11] and/or pressure,[12] or by ball milling[13] is of particular interest. Here, we make it clear that we refer to the general noncrystalline ZIF as amorphous ZIF (a-ZIF), whereas experimentally obtained ZIFs are ZIF glass or a-ZIF glass, although the terms are used interchangeably in other literature. The a-ZIF can be viewed as a model system for understanding the general features and properties of a novel hybrid inorganic/organic glass with no long-range order (LRO) but with well-preserved short-range order (SRO). Recently, there has been increased interest in the structure of ZIF glasses subject to elevated temperatures near the crystalline to amorphous phase transition.[10] Experimentally, the complex temperature-dependent behaviors of ZIF glasses have been characterized with advanced techniques such as X-ray diffraction, neutron diffraction, Raman and Brillouin spectroscopy,[10,11,14] and positron annihilation lifetime spectroscopy (PALS).[15] Simultaneously, there has been a steady increase in the number of theoretical studies using molecular dynamic (MD) simulations[16,17] and ab initio calculations.[14,18−20] Despite these efforts, the mechanism of ZIF glass formation on the basis of detailed interatomic interactions is not fully understood.

The main shortcoming encountered in the computational studies appears to be that while the presence of SRO has been predicted,[11] there remains an inability to precisely quantify the intermediate-range order (IRO) with distances of separation in the range of 10−20 Å and to verify the absence of LOR. The reason for that problem is the lack of realistic a-ZIF models of sufficiently large size. Furthermore, the a-ZIF models derived from different MD simulations depend on the methods and potentials used as well as the starting configurations, which can result in significant uncertainty in the IRO due in part to the possibility of defect structures. The defect structures often distort any physical properties that are calculated based on such models. Therefore, it is highly desirable to first construct a sufficiently large but also nearly perfect continuous random

Received: June 22, 2016
Published: June 26, 2016

DOI: 10.1021/acs.jpcc.6b06337
J. Phys. Chem. C 2016, 120, 15362−15368

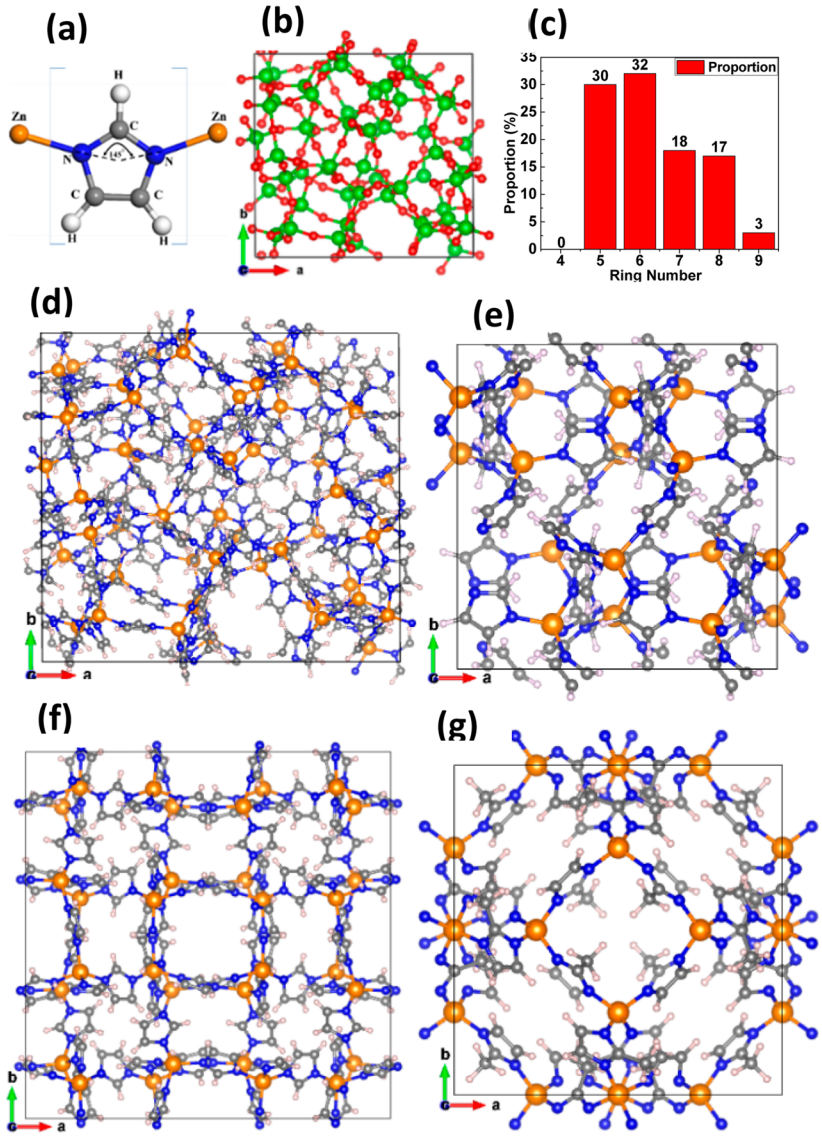

Figure 1. (a) Zn−IM−Zn unit of ZIFs, (b) 162 atom a-SiO_2 model, and (c) ring statistics of the a-SiO_2 model. Ball and stick figures of (d) a-ZIF model, (e) ZIF-4 crystal, (f) ZIF-zni crystal, and (g) ZIF-8 crystal. Orange, blue, gray, and white balls represent Zn, N, C, and H respectively.

network (CRN) model of a-ZIF to serve as a baseline for comparative studies. Here we report the construction and characterization of a near-perfect CRN model for a-ZIF with periodic boundaries obtained through the conversion of a special a-SiO_2 model that was generated from our previous work. We then calculate the electronic structure, interatomic bonding, and optical properties of this defect-free a-ZIF model (Figure 1d). Also reported are the results of parallel calculations of three crystalline ZIFs, ZIF-4, ZIF-zni, and ZIF-8 (Figure 1e−g). The electronic structure and bonding of a-ZIF and the crystalline ZIFs are very similar because they share the same SRO. We also find that substantial Zn−N bond strength is the key for the integrity of the a-ZIF network. The calculated optical properties of a-ZIF show interesting absorption features, a low index of refraction (1.327), and a plasmon frequency of 15.81 eV.

METHODS

The computational methods for model optimization, analysis, and properties' calculations are presented in detail in the Supporting Information (SI). The modeling strategy and process for a-ZIF is described below.

The a-ZIF model presented here originates from a 162 atom periodic a-SiO_2 model (54 SiO_2 molecules) (Figure 1b) constructed 35 years ago.[21] The beauty of this model is that it has near-perfect local bonding with no over- or under-coordinated Si or O atoms and a realistic distribution of four-, five-, six-, seven-, eight-, and nine-membered rings (Figure 1c), which is extremely difficult to construct across the periodic boundary due to strong directional Si−O bonds. Such a near-perfect CRN model cannot be obtained by using MD. This model has no four-member rings and contains mostly five- and six-membered rings (30 and 32%), considerable seven- and eight-membered rings (18 and 17%), and a small presence of nine-membered rings (3%). The distribution of rings indicates that this is a truly CRN model of silica even with the absence of four-membered rings. This a-SiO_2 model was originally obtained from a carefully built periodic model of amorphous Si[22] by inserting O atoms at the middle of the Si−Si bonds and rescaling the cell size. Over the years, the model has been systematically improved, enlarged, and used as a representative

DOI: 10.1021/acs.jpcc.6b06337
J. Phys. Chem. C 2016, 120, 15362−15368

model for a-SiO_2 to calculate many different properties,[23−25] including amorphous to amorphous phase transition under pressure.[26] The initial a-ZIF structure had the same network topology as the a-SiO_2 model and was then fully relaxed with high accuracy. The resulting periodic a-ZIF model had a total of 918 atoms (Figure 1d). Details about the conversion and optimization of the model are described in the SI. A similar a-ZIF model was reported[11] from a larger a-SiO_2 model[27] following the same approach of using an a-Si model.[28] However, the original a-Si model used in that work started from the crystalline diamond structure, and it contained very different ring statistics. The a-SiO_2 model of ref 27 was used to obtain an a-ZIF model using the reverse Monte Carlo (RMC) technique.[27] However, the resulting model contained defective sites, making the conversion to an ideal network of a-ZIF model difficult. The present a-ZIF model that we constructed has no such defects and is of appropriate size for relatively easy application of ab initio electronic structure methods. Moreover, the differently sized ring structures are the source of the large distribution of different pores in MOF glasses, as observed in PALS.[15]

RESULTS

In this section, we first analyze the structure of a-ZIF and then show the electronic structure properties and optical properties. The radial distribution function (RDF) $g(r)$ of the a-ZIF model was calculated with the Interactive Structure Analysis of Amorphous and Crystalline systems (ISAACS) program[29] and compared to experimentally measured data $G(r)$ from ZIF glass a_T-ZIF-4[30] (Figure 2a,b). The experimental data was obtained from the Fourier transform of the total scattering function $S(Q)$ produced from X-ray total scattering data. The experimental spectrum does not show peaks A′ and E′ present in Figure 2b because they involve H atoms. However, all others peaks in the computed and experimental data align well. We take this as an indication that our a-ZIF model fits well with the experimental data for the a_T-ZIF-4; both clearly show evidence of the retention of SRO and IRO through the major peaks below 6 Å and the lack of LRO beyond 6 Å. The peak at 6 Å is due to the Zn−Zn pairs. Contrary to experimental RDF $G(r)$ based on scattering factor $S(Q)$, which is incapable of identifying light H atoms, the calculated RDF $g(r)$ from the a-ZIF model contains all information of partial RDF (PRDF) of all atomic pairs (Figure 2c), including H, which has a significant effect on the locations and shapes of the peaks shown in Figure 2b. There are seven prominent structures in $g(r)$ (marked A′, A, B, C, D, E′, and E). The sharp peaks from H-related pairs in the a-ZIF model are the results of the large number of H atoms in the a-ZIF model. For instance, the first very sharp peak A′ in $g(r)$ comes from the enormous number of C−H pairs.

The compositions of the other peaks are (A) C−N, C−C; (B) Zn−N, C−C, N−H, N−C, N−N, C−H; (C) Zn−C, Zn−H, N−N, C−H, N−H, H−H; (D) Zn−N, Zn−C, H−H; (E′) Zn−H; and (E) Zn−Zn. Moreover, the experimental data cannot resolve the difference between C−C and C−N bonds, but the PRDF clearly shows their relative contributions. Other details of the a-ZIF model (including calculated properties to be described below) and those of the three crystalline phases, ZIF-4, ZIF-zni, and ZIF-8 (solvent-free), are summarized in Table 1. We note that a-ZIF has a much lower density than ZIF-4 and ZIF-zni but that it has a higher density than ZIF-8 due to the presence of large pores in ZIF-8.

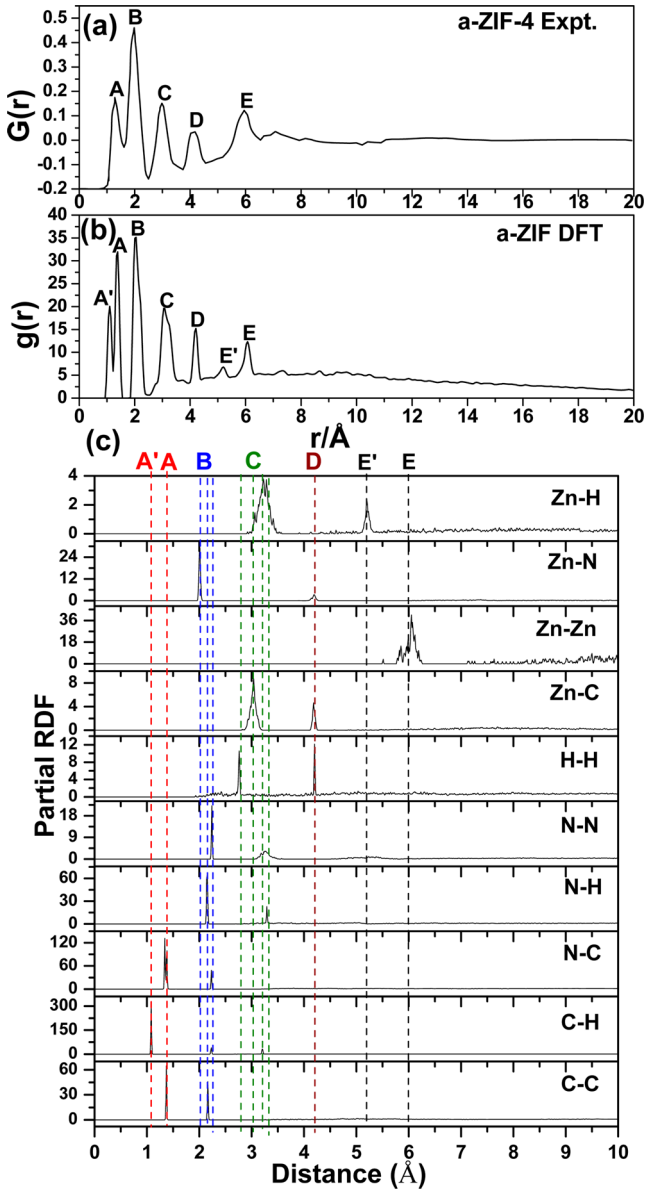

Figure 2. (a) Experimental RDF of the a-ZIF-4, (b) RDF for the present a-ZIF model, and (c) PRDF for all atomic pairs for the a-ZIF model.

Despite numerous theoretical calculations on crystalline and amorphous ZIFs, it is intriguing to note that results on the electronic structure are somehow missing. We have calculated electronic structure and interatomic bonding information for the a-ZIF model using the ab initio orthogonalized linear combination of atomic orbitals (OLCAO) method.[31] (More details on the OLCAO calculation are given in the SI.) The calculated total density of states (TDOS) and partial DOS (PDOS) of a-ZIF are shown in Figure 3a. A large band gap of 4.8 eV, which may be underestimated due to the usual deficiency of LDA-based DFT methods, indicates that a-ZIF is an insulator. From the TDOS, the occupied portion of the valence band (VB) consists of nearly all sharp peaks, that is, two very sharp peaks (A and B), four relatively sharp peaks (C−F) in the lower VB, three broader peaks (G−I) in the lower part of the upper VB, and four broader peaks (J−M) in the upper part of the upper VB. In the unoccupied conduction band (CB) region, there is only one prominent peak (N) at 6.0

DOI: 10.1021/acs.jpcc.6b06337
J. Phys. Chem. C 2016, 120, 15362−15368

Table 1. Structure of the a-ZIF Model and the ZIF-4, ZIF-zni, and ZIF-8 Crystals

ZIFs	a-ZIF	ZIF-4	ZIF-zni	ZIF-8
chemical composition	$Zn_{54}N_{216}C_{324}H_{324}$	$Zn_{16}N_{64}C_{96}H_{96}$	$Zn_{32}N_{128}C_{192}H_{192}$	$Zn_{12}N_{48}C_{96}H_{120}$
a, *b*, *c* (Å)	26.729, 24.417, 27.645	15.316, 15.577, 18.584	23.802(23.503), 23.802(23.503), 12.595(12.461)	17.140, 17.139, 17.139
α, *β*, *γ*	90.73°, 93.66°, 90.21°	90°, 90°, 90°	90°, 90°, 90°	90°,90°, 90°
space group	1	*Pbca*	*I*41*cd*	$I\bar{4}3m$
V (nm^3)	18.00	4.43	7.14	5.03
E_0 (eV)	−6023.11	−1786.12	−3572.22	−1740.46
E_0 (kJ/mol)	−581141.23	−172334.14	−344666.36	−167928.82
E_0[a](kJ/mol)/ tetra. site	−10761.87	−10770.88	−10770.82	−13994.07
density[b] nm^{-3}	3.00	3.61	4.48	2.38
mass density (amu/$Å^3$)	0.60	0.73	0.90	0.55

[a]E_0 is the total energy of the respective ZIF models in units of eV and also in kJ/mol per tetrahedral site. [b]Densities are expressed as the number of tetrahedral sites per unit volume.

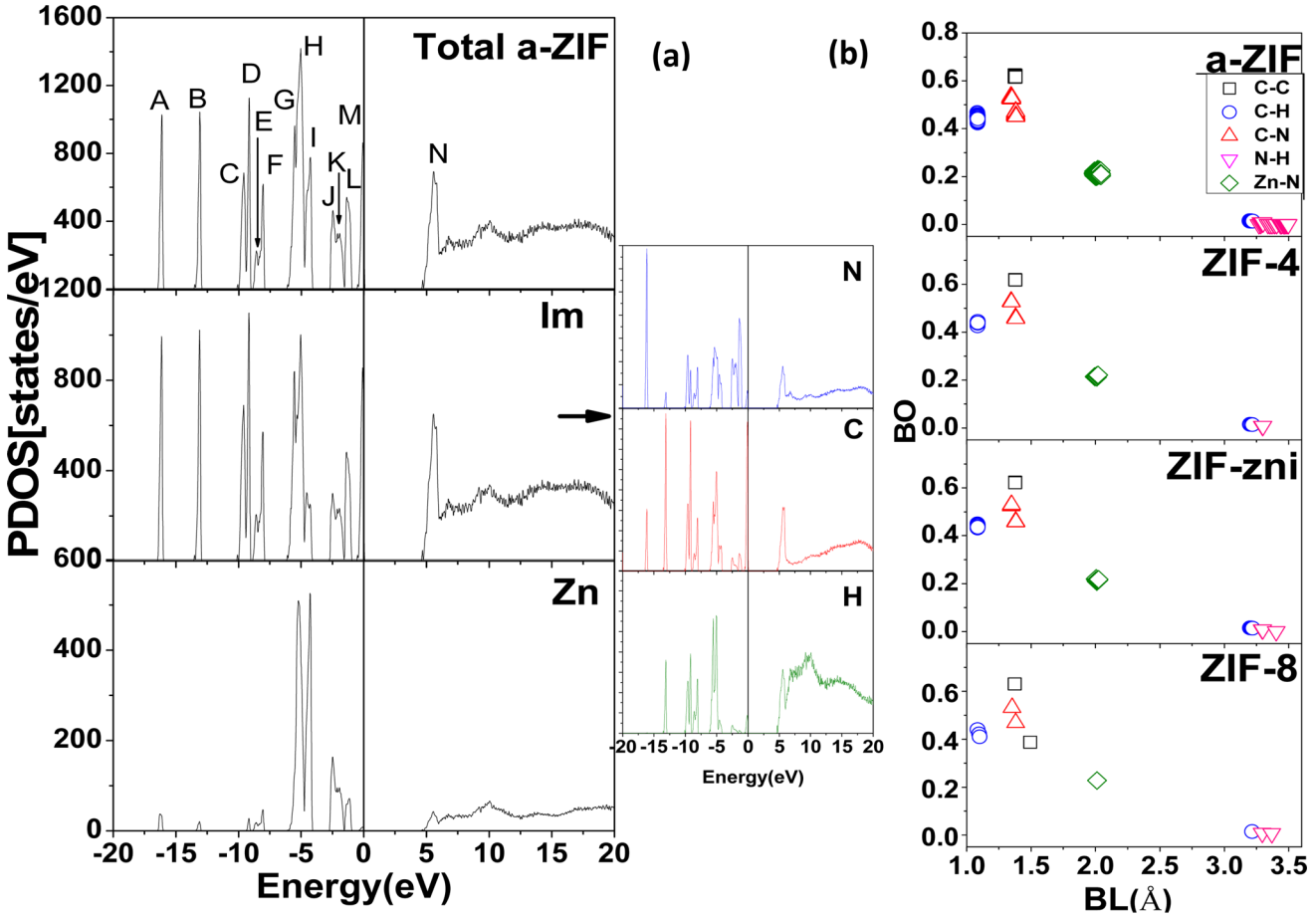

Figure 3. (a) Calculated TDOS and PDOS of a-ZIF and (b) BO versus BL plots of a-ZIF, ZIF-4, ZIF-zni, and ZIF-8. The sidebar to (a) depicts the PDOS of the different types of bonds in Im.

eV followed by a plateau to which all of the atoms contribute. The PDOS also provides insight regarding the interatomic bonding in a-ZIF. For example, above −6 eV, the Zn atoms interact strongly with N and H atoms. All of these data indicate that the electronic structure of a-ZIF bears a strong resemblance to the broadened spectrum of the organic molecule IM. The PDOS for crystalline ZIF-4, ZIF-zni, and ZIF-8 are shown in Figure S1 in the SI.

To characterize the nature of the bonding and charge transfer in a-ZIF, we have calculated the effective charge Q* and bond order (BO) values according to eq 1 in the SI. They are listed in Table 2. Figure 3b shows the distribution of the calculated BO versus bond length (BL) up to 4 Å, which provides basic bonding information in a-ZIF. The narrow distributions of C−C, C−H, N−C, and Zn−N pairs in both a-ZIF and crystalline ZIFs are almost identical, which indicates that the SRO in the a-ZIF model remains the same as that in the crystalline phases. The average BO for N−H pairs is negligible. The C−N bonds have two kinds of BO values due to the two types of covalent C−C bonds in the IM ring (one is stronger than the other). It also shows two types of C−C bonding in ZIF-8 corresponding to C−C bonding in the substituted CH_3 group in methylimidazolate, which is different from the C−C bond in IM. In all ZIFs, the highest BO values are those of the strongly

DOI: 10.1021/acs.jpcc.6b06337
J. Phys. Chem. C 2016, 120, 15362−15368

Table 2. Calculated Total and Partial BOD, Effective Charge Q*, and Physical Parameters in a-ZIF and Three ZIF Crystals

type/PBOD	a-ZIF	ZIF-4	ZIF-zni	ZIF-8
C−C	0.0037	0.0045	0.0056	0.0049
C−H	0.0082	0.0098	0.0123	0.0103
C−N	0.0118	0.0143	0.0177	0.0096
Zn−N	0.0026	0.0031	0.0039	0.0022
TBOD	0.0264	0.0318	0.0396	0.0270
E_g	4.673	5.134	4.840	4.574
n	1.327	1.367	1.460	1.311
average Q^*				
C	4.086	4.087	4.081	4.178
N	5.453	5.453	5.449	5.411
H	0.761	0.759	0.767	0.779
Zn	11.105	11.114	11.114	11.139
ε_2 peaks (eV)				
A1	5.590	5.490	5.480	5.410
A2	6.800	6.750	6.630	6.590
ω_p (eV)	15.810	16.930	17.280	16.120

covalent C−C bonds, followed by the C−N bonds. The short C−H bonds (1.085 Å) have slightly smaller BO values than those of the C−C and C−N bonds. The C−H bonds are slightly weaker because H atoms are outside of the IM ring. The slightly larger variance in C−H bonds in ZIF-8 is because some of the bonds are from methylimidazolate, which has a different local environment. In all four ZIFs, Zn connects with IM via N bonding with a relatively large BO value and a BL close to 2.0 Å. This is the key for maintaining the near-perfect tetrahedral Zn−N_4 tetrahedral bonding with IM or methylimidazolate.

Table 2 also lists the calculated total bond order density (TBOD) and partial BOD (PBOD) (see the SI), band gap (E_g), refractive index (to be discussed below), and average effective charge Q^* of the ZIFs. TBOD is a single quantum mechanical metric obtained from electronic structure calculations and that reflects the internal cohesion of complex materials[32] ideal for assessing material properties in both crystalline and noncrystalline solids. In many cases, the TBOD is more reliable and convenient than the total energy or formation energy because it is independent of the cell size. The calculated TBOD for a-ZIF is 0.0264 $e^-/Å^3$, which is smaller than that of its crystalline counterparts. ZIF-4 and ZIF-zni have a TBOD of 0.0317 and 0.0396 $e^-/Å^3$, respectively. This indicates that the crystalline phases have a higher internal cohesion than the amorphous phase even though their SROs are identical. However, the TBOD for ZIF-8 of 0.0276 $e^-/Å^3$ is close to that of a-ZIF, indicating a much weaker internal cohesion than ZIF-4 or ZIF-zni and can be attributed to the large porosity in ZIF-8.

MOF materials are envisioned to have many as of yet unrealized applications as functional materials.[33−36] We have calculated the optical properties for a-ZIF within one-electron DFT in the form of the frequency-dependent complex dielectric function (see the SI for detail). We are not aware of any previous investigation of the optical properties of any ZIF materials except for some recent work on infrared and Raman spectra related to vibrations at very low frequencies.[37] Figure 4 shows the calculated frequency-dependent complex dielectric function and the electron energy loss function (ELF) as a function of photon energies up to 35 eV for a-ZIF based on

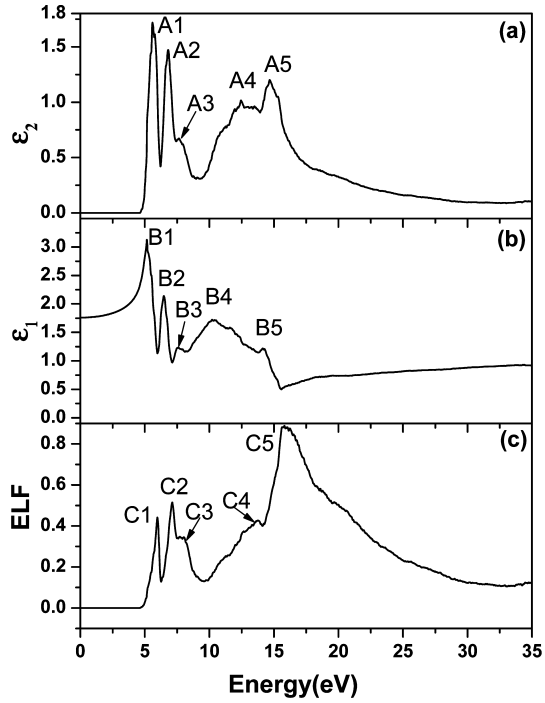

Figure 4. Optical properties of a-ZIF. (a) Imaginary dielectric function ε_2. (b) Real part of the dielectric function ε_1. (c) ELF.

eqs 2−4 (see the SI). Ab initio optical properties calculation of the a-ZIF model with 918 atoms is computationally very challenging. There are five prominent features (A1−A5) that carry over from $\varepsilon_2(\omega)$ to $\varepsilon_1(\omega)$ (B1−B5) and then to the ELF (C1−C5), with the largest peak C5 at 15.810 eV identified as the plasmon peak ω_p for collective oscillations of the electrons in a-ZIF. The optical properties of crystalline ZIF-4, ZIF-zni, and ZIF-8 are shown in Figure S2 in the SI together with a-ZIF. The overall features are similar to those of a-ZIF but with sharper absorption peaks due to their crystalline nature with LRO. We note the rather sensitive variations in the shape and the location of the plasmon peak ω_p, which should be easily detectable experimentally. Most importantly, the refractive indices n for the four ZIF systems were obtained from the square root of $\varepsilon_1(\omega)$ at zero frequency (excluding the vibrational effect) and were found to be 1.327, 1.367, 1.460, and 1.311 for a-ZIF, ZIF-4, ZIF-zni, and ZIF-8, respectively. The smaller value of n for ZIF-8 compared to that of a-ZIF is likely due to its higher porosity and low density. It is possible to correlate the ultralow refractive index of ZIF materials to their porosity if they could be measured with sufficient accuracy. We also speculate that n could be a convenient and measurable descriptor for characterizing a-ZIF films. The peak positions in the absorption curves and the position of ω_p in the four ZIF systems are listed in Table 2.

CONCLUSIONS

In summary, we have shown the following: (1) A near-perfect CRN model for a-ZIF that was not derived from a crystalline phase has been constructed with RDF in good agreement with measurement. (2) The electronic structure and bonding for the a-ZIF are elucidated in great detail showing considerable bond strength in the Zn−N pairs. Very similar results were obtained for the three ZIF crystals, ZIF-4, ZIF-zni, and ZIF-8, reaffirming the identical atomic scale SRO. (3) The optical properties of a-

DOI: 10.1021/acs.jpcc.6b06337
J. Phys. Chem. C 2016, 120, 15362−15368

ZIF were calculated showing unique absorption features and an ultralow refractive index of 1.327. These and other properties are critically compared with three other crystalline ZIF phases. Their sensitive dependence on the structures can be used to characterize and predict the different types of ZIF phases, especially in relation to their porosity and thus their ability to encapsulate other molecules.

■ ASSOCIATED CONTENT

Supporting Information

The Supporting Information is available free of charge on the ACS Publications website at DOI: 10.1021/acs.jpcc.6b06337.

Additional computational details; construction and optimization of the a-ZIF model; and electronic structure calculations of the a-ZIF model using OLCAO (PDF)

■ AUTHOR INFORMATION

Corresponding Authors

*E-mail: lineng@whut.edu.cn (N.L.).
*E-mail: Chingw@umkc.edu (W.-Y.C.).

Notes

The authors declare no competing financial interest.

■ ACKNOWLEDGMENTS

We thank Prof. Yuanzheng Yue and Dr. Thomas Bennett for very helpful discussions. Work at UMKC is partially supported by the UMKC research incentive fund. We used the resources of the National Energy Research Scientific Computing Center supported by the DOE under Contract No. DE-AC03-76SF00098 and the UM bioinformatics consortium computing facility. Work at WUT was supported by the Natural Science Foundation of Hubei Province with Contract No. 2015CFB227, by the Scientific Research Foundation for the Returned Overseas Chinese Scholars with Contract No. [2015] 0303, the Fundamental Research Funds for the Central Universities (WUT: 2015-IVA-051), the research board of the State Key Laboratory of Silicate Materials for Architectures, and the Wuhan University of Technology (Contract No. 47152005).

■ REFERENCES

(1) Rao, C.; Cheetham, A.; Thirumurugan, A. Hybrid inorganic–organic materials: a new family in condensed matter physics. *J. Phys.: Condens. Matter* **2008**, *20* (8), 083202.

(2) Férey, G. Some suggested perspectives for multifunctional hybrid porous solids. *Dalton Transactions* **2009**, *23*, 4400–4415.

(3) Furukawa, H.; Cordova, K. E.; O'Keeffe, M.; Yaghi, O. M. The chemistry and applications of metal-organic frameworks. *Science* **2013**, *341* (6149), 1230444.

(4) Mondloch, J. E.; Katz, M. J.; Isley, W. C., III; Ghosh, P.; Liao, P.; Bury, W.; Wagner, G. W.; Hall, M. G.; DeCoste, J. B.; Peterson, G. W.; et al. Destruction of chemical warfare agents using metal–organic frameworks. *Nat. Mater.* **2015**, *14* (5), 512–516.

(5) Banerjee, R.; Phan, A.; Wang, B.; Knobler, C.; Furukawa, H.; O'Keeffe, M.; Yaghi, O. M. High-throughput synthesis of zeolitic imidazolate frameworks and application to CO2 capture. *Science* **2008**, *319* (5865), 939–943.

(6) Tran, U. P.; Le, K. K.; Phan, N. T. Expanding applications of metal– organic frameworks: zeolite imidazolate framework ZIF-8 as an efficient heterogeneous catalyst for the knoevenagel reaction. *ACS Catal.* **2011**, *1* (2), 120–127.

(7) Tian, Y. Q.; Cai, C. X.; Ren, X. M.; Duan, C. Y.; Xu, Y.; Gao, S.; You, X. Z. The Silica-Like Extended Polymorphism of Cobalt (II) Imidazolate Three-Dimensional Frameworks: X-ray Single-Crystal Structures and Magnetic Properties. *Chem. - Eur. J.* **2003**, *9* (22), 5673–5685.

(8) Liu, S.; Xiang, Z.; Hu, Z.; Zheng, X.; Cao, D. Zeolitic imidazolate framework-8 as a luminescent material for the sensing of metal ions and small molecules. *J. Mater. Chem.* **2011**, *21* (18), 6649–6653.

(9) Bennett, T. D.; Tan, J.-C.; Yue, Y.; Baxter, E.; Ducati, C.; Terrill, N. J.; Yeung, H. H.-M.; Zhou, Z.; Chen, W.; Henke, S.; et al. Hybrid glasses from strong and fragile metal-organic framework liquids. *Nat. Commun.* **2015**, *6*, 8079.

(10) Bennett, T. D.; Yue, Y.; Li, P.; Qiao, A.; Tao, H.; Greaves, N. G.; Richards, T.; Lampronti, G. I.; Redfern, S. A.; Blanc, F.; et al. Melt-Quenched Glasses of Metal-Organic Frameworks. *J. Am. Chem. Soc.* **2016**, *138* (10), 3484–3492.

(11) Bennett, T. D.; Goodwin, A. L.; Dove, M. T.; Keen, D. A.; Tucker, M. G.; Barney, E. R.; Soper, A. K.; Bithell, E. G.; Tan, J.-C.; Cheetham, A. K. Structure and properties of an amorphous metal-organic framework. *Phys. Rev. Lett.* **2010**, *104* (11), 115503.

(12) Bennett, T. D.; Simoncic, P.; Moggach, S. A.; Gozzo, F.; Macchi, P.; Keen, D. A.; Tan, J.-C.; Cheetham, A. K. Reversible pressure-induced amorphization of a zeolitic imidazolate framework (ZIF-4). *Chem. Commun.* **2011**, *47* (28), 7983–7985.

(13) Bennett, T. D.; Cao, S.; Tan, J. C.; Keen, D. A.; Bithell, E. G.; Beldon, P. J.; Friscic, T.; Cheetham, A. K. Facile mechanosynthesis of amorphous zeolitic imidazolate frameworks. *J. Am. Chem. Soc.* **2011**, *133* (37), 14546–14549.

(14) Baxter, E. F.; Bennett, T. D.; Mellot-Draznieks, C.; Gervais, C.; Blanc, F.; Cheetham, A. K. Combined experimental and computational NMR study of crystalline and amorphous zeolitic imidazolate frameworks. *Phys. Chem. Chem. Phys.* **2015**, *17* (38), 25191–25196.

(15) Thornton, A. W.; Jelfs, K. E.; Konstas, K.; Doherty, C.; Hill, A.; Cheetham, A.; Bennett, T. D. Porosity in metal–organic framework glasses. *Chem. Commun.* **2016**, *52*, 3750.

(16) Gao, M.; Misquitta, A. J.; Rimmer, L. H. N.; Dove, M. T. Molecular dynamics simulation study of various zeolitic imidazolate framework structures. *Dalton Transactions* **2016**, *45* (10), 4289–4302.

(17) du Bourg, L. B.; Ortiz, A. U.; Boutin, A.; Coudert, F.-X. Thermal and mechanical stability of zeolitic imidazolate frameworks polymorphs. *APL Mater.* **2014**, *2* (12), 124110.

(18) Tan, J.-C.; Civalleri, B.; Erba, A.; Albanese, E. Quantum mechanical predictions to elucidate the anisotropic elastic properties of zeolitic imidazolate frameworks: ZIF-4 vs. ZIF-zni. *CrystEngComm* **2015**, *17* (2), 375–382.

(19) Ryder, M. R.; Tan, J.-C. Explaining the mechanical mechanisms of zeolitic metal–organic frameworks: revealing auxeticity and anomalous elasticity. *Dalton Transactions* **2016**, *45* (10), 4154–4161.

(20) Ortiz, A. l. U.; Boutin, A.; Gagnon, K. J.; Clearfield, A.; Coudert, F. o.-X. Remarkable Pressure Responses of Metal–Organic Frameworks: Proton Transfer and Linker Coiling in Zinc Alkyl Gates. *J. Am. Chem. Soc.* **2014**, *136* (32), 11540–11545.

(21) Ching, W. Microscopic calculation of localized electron states in an intrinsic glass. *Phys. Rev. Lett.* **1981**, *46* (9), 607.

(22) Guttman, L.; Ching, W.; Rath, J. Charge-density variation in a model of amorphous silicon. *Phys. Rev. Lett.* **1980**, *44* (23), 1513.

(23) Huang, M.-Z.; Ching, W. Electron states in a nearly ideal random-network model of amorphous SiO 2 glass. *Phys. Rev. B: Condens. Matter Mater. Phys.* **1996**, *54* (8), 5299.

(24) Huang, M.-Z.; Ouyang, L.; Ching, W. Electron and phonon states in an ideal continuous random network model of a– SiO 2 glass. *Phys. Rev. B: Condens. Matter Mater. Phys.* **1999**, *59* (5), 3540.

(25) Li, N.; Ching, W.-Y. Structural, electronic and optical properties of a large random network model of amorphous SiO 2 glass. *J. Non-Cryst. Solids* **2014**, *383*, 28–32.

(26) Li, N.; Sakidja, R.; Aryal, S.; Ching, W.-Y. Densification of a continuous random network model of amorphous SiO 2 glass. *Phys. Chem. Chem. Phys.* **2014**, *16* (4), 1500–1514.

(27) Tucker, M.; Keen, D.; Dove, M.; Trachenko, K. Refinement of the Si–O–Si bond angle distribution in vitreous silica. *J. Phys.: Condens. Matter* **2005**, *17* (5), S67.

DOI: 10.1021/acs.jpcc.6b06337
J. Phys. Chem. C 2016, 120, 15362–15368

(28) Wooten, F.; Winer, K.; Weaire, D. Computer generation of structural models of amorphous Si and Ge. *Phys. Rev. Lett.* **1985**, *54* (13), 1392.
(29) Le Roux, S.; Petkov, V. ISAACS—interactive structure analysis of amorphous and crystalline systems. *J. Appl. Crystallogr.* **2010**, *43* (1), 181—185.
(30) Bennett, T. D.; Cheetham, A. K. Amorphous Metal—Organic Frameworks. *Acc. Chem. Res.* **2014**, *47* (5), 1555—1562.
(31) Ching, W.-Y.; Rulis, P. *Electronic Structure Methods for Complex Materials: The orthogonalized linear combination of atomic orbitals*; Oxford University Press, 2012.
(32) Dharmawardhana, C.; Misra, A.; Ching, W.-Y. Quantum mechanical metric for internal cohesion in cement crystals. *Sci. Rep.* **2014**, *4*, 7332.
(33) Horcajada, P.; Serre, C.; Vallet-Regí, M.; Sebban, M.; Taulelle, F.; Férey, G. Metal—organic frameworks as efficient materials for drug delivery. *Angew. Chem.* **2006**, *118* (36), 6120—6124.
(34) Zacharia, R.; Cossement, D.; Lafi, L.; Chahine, R. Volumetric hydrogen sorption capacity of monoliths prepared by mechanical densification of MOF-177. *J. Mater. Chem.* **2010**, *20* (11), 2145—2151.
(35) Kreno, L. E.; Leong, K.; Farha, O. K.; Allendorf, M.; Van Duyne, R. P.; Hupp, J. T. Metal—organic framework materials as chemical sensors. *Chem. Rev.* **2012**, *112* (2), 1105—1125.
(36) Pimentel, B. R.; Parulkar, A.; Zhou, E. k.; Brunelli, N. A.; Lively, R. P. Zeolitic Imidazolate Frameworks: Next-Generation Materials for Energy-Efficient Gas Separations. *ChemSusChem* **2014**, *7* (12), 3202—3240.
(37) Tanaka, S.; Fujita, K.; Miyake, Y.; Miyamoto, M.; Hasegawa, Y.; Makino, T.; Van der Perre, S.; Cousin Saint Remi, J.; Van Assche, T.; Baron, G. V.; et al. Adsorption and Diffusion Phenomena in Crystal Size Engineered ZIF-8 MOF. *J. Phys. Chem. C* **2015**, *119* (51), 28430—28439.

DOI: 10.1021/acs.jpcc.6b06337
J. Phys. Chem. C 2016, 120, 15362—15368